High-Performance Separation of Nanoparticles with Ultrathin Porous Nanocrystalline Silicon Membranes

Thomas R. Gaborski,[†,§] Jessica L. Snyder,[‡] Christopher C. Striemer,[§,⊥] David Z. Fang,[⊥] Michael Hoffman,[†] Philippe M. Fauchet,[⊥] and James L. McGrath[†,*]

[†]Department of Biomedical Engineering, University of Rochester, Rochester, New York 14627, United States, [‡]Department of Biochemistry and Biophysics, University of Rochester, Rochester, New York 14627, United States, [§]SiMPore Inc., West Henrietta, New York 14586, United States, and [⊥]Department of Electrical and Computer Engineering, University of Rochester, Rochester, New York 14627, United States

ABSTRACT Porous nanocrystalline silicon (pnc-Si) is a 15 nm thin free-standing membrane material with applications in small-scale separations, biosensors, cell culture, and lab-on-a-chip devices. Pnc-Si has already been shown to exhibit high permeability to diffusing species and selectivity based on molecular size or charge. In this report, we characterize properties of pnc-Si in pressurized flows. We compare results to long-standing theories for transport through short pores using actual pore distributions obtained directly from electron micrographs. The measured water permeability is in agreement with theory over a wide range of pore sizes and porosities and orders of magnitude higher than those exhibited by commercial ultrafiltration and experimental carbon nanotube membranes. We also show that pnc-Si membranes can be used in dead-end filtration to fractionate gold nanoparticles and protein size ladders with better than 5 nm resolution, insignificant sample loss, and little dilution of the filtrate. These performance characteristics, combined with scalable manufacturing, make pnc-Si filtration a straightforward solution to many nanoparticle and biological separation problems.

KEYWORDS: purification · thin film · semiconductor · microfluidics · nanofluidics

The need to physically separate similarly sized solutes is a ubiquitous problem in biological research and in the production of biomolecules and other nanoparticles. Compared to resin-based chromatography, membrane separations are simpler, more energy efficient, and more readily scaled between laboratory and industry.[1] Fundamental advances in membrane technology that impact the efficiency of ultrafiltration processes can lower drug and food costs, accelerate the process of discovery in biological laboratories, and enable new devices such as wearable blood dialysis systems. While membrane-based bind and elute strategies such as ion exchange and affinity methods have advanced significantly in recent years,[2−4] size-exclusion chromatography, the most robust method for separating similarly sized macromolecules, still has no commonly used membrane analogue. Ideally, a nanoporous membrane could be used as a sieve to precisely fractionate a mixture of nanoparticles forced through the membrane with little dilution or contamination of the filtrate.

Traditional ultrafiltration membranes, made from solvent-casted polymers, have tortuous path, sponge-like, pore structures that limit the resolution of separations. Such membranes are typically used to separate materials that are orders of magnitude different in size in dialysis, solute concentration, and buffer exchanges. The membranes are also micrometers thick and highly porous, giving more than 100 μm^2 of internal surface area for every μm^2 of frontal surface.[5] High internal surface area leads to flow resistance, sample loss, and clogging in flow-through filtration systems. Experimental thin (∼50−100 nm) tortous path membranes made from cross-linked proteins[6] or polymers[6] have pore size cut-offs appropriate for nanofiltration (<2 nm) rather than ultrafiltration (2−50 nm).[7]

To create idealized membranes for size-based separations, technologists have developed nanoporous membranes with well-defined and tunable pore sizes. Aluminum oxide and track-etched membranes are commercially available examples, but the pores in these membranes are too large (>20 nm) for many biological separations. In addition, these membranes are very thick (6−10 μm) so that transport is too slow for many purification processes.[8] Silicon patterning techniques have been used to create membranes with uniform 10 nm wide pores,[9] but the thickness (4 μm) and low porosity (∼1%) of these membranes again limit transport. Flow through membranes created from aligned carbon nanotubes (CNTs) has been shown to exceed the predictions of viscous flow theory because of the smooth and hydrophobic walls of CNTs;

*Address correspondence to jmcgrath@bme.rochester.edu.

Received for review August 17, 2010 and accepted October 25, 2010.

Published online November 2, 2010. 10.1021/nn102064c

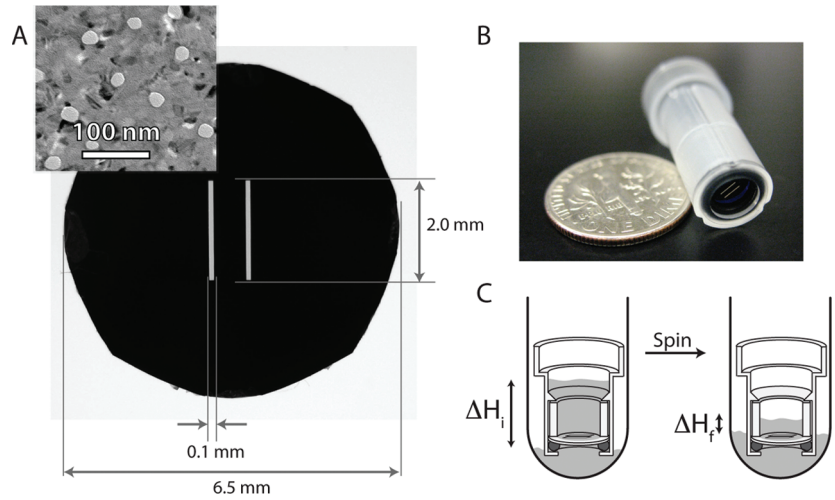

Figure 1. (A) Circular pnc-Si chip formatted for plastic centrifuge tube inserts. The two internal slits are areas of free-standing pnc-Si membrane. Inset: TEM micrograph of pnc-Si membranes. Pores are white, and nanocrystals are black. (B) Assembled centrifuge tube insert. (C) Schematic of hydraulic permeability test. The insert is filled with water and placed in a larger collection tube prefilled with water. The system is spun in a centrifuge, and the volume of water that passes through the membrane is measured. Hydraulic permeability measurements are taken before the system reaches equilibrium.

however, the pore sizes are limited to a small range between 2 and 6 nm that depends on the particular CNT formulation used. Ultrathin silicon membranes (~10 nm) with defined pores (25 nm) were first created using an ion-beam drilling process that is far too slow for scale up.[10] Recently, track-etched technology has been applied to SiN membranes to create 100 nm thick membranes with pore sizes that can be tuned between ~10 and 50 nm depending on the time allotted to etching;[11] however, this technique requires access to a cyclotron capable of heavy ion (Bi, Xe) bombardment and thus also faces high volume manufacturing challenges.

Here we examine the pressurized flow and filtration properties of ultrathin porous nanocrystalline silicon (pnc-Si). Pnc-Si is a recently developed material created by crystallizing a thin amorphous silicon film to produce nanometer-sized voids that become through-pores.[12] The membranes are mass-produced on silicon wafers using standard microfabrication tools and processes. Free-standing membranes as thin as 15 nm have been shown to withstand up to an atmosphere of pressure without mechanical failure. Pore distributions exhibit sharp cut-offs that can be tuned between 5 and 80 nm by changing the annealing temperature during fabrication.[12] In contrast to polymer membranes, pnc-Si membranes have ~0.1 μm^2 of internal surface area for every um^2 of frontal surface. Fast diffusion and molecular separations with pnc-Si have already been demonstrated for small solutes;[12,13] however, the use of pnc-Si membranes as flow-through filters has not been previously investigated.

RESULTS AND DISCUSSION

We examined the hydraulic permeability of pnc-Si membranes using bucket-style devices resembling those commonly used for concentrating nanomaterials (Figure 1). The devices housed 6.5 mm diameter silicon membrane chips with free-standing membranes over two 2 mm × 0.1 mm windows (Figure 1A). Water was forced through the membranes in a centrifuge. Interestingly, the membranes were found to be impermeable to water unless both sides of the membrane were wet (discussed below), so water was also added to the outer test tube to immerse the membrane. The difference in water levels between the inside and outside containers creates a pressure drop across the membrane that diminishes over time (Figure 1C). Fluid volumes in both containers were determined by weighing samples at different time points, and the hydraulic permeability was determined by fitting data to a formula that describes the evolution of fluid levels in both containers (see Supporting Information).

We compared water flow rates through pnc-Si to a formula derived by Dagan *et al.*[14] describing low Reynolds number flow through short pores accounting for entrance, exit, and tube resistances (see Supporting Information). We used custom image processing routines (Figure S1) to determine the distribution of pore sizes in a transmission electron micrograph (Figure 2A) and then used the Dagan formula to calculate the predicted water flow through each pore in the micrograph. The theoretical hydraulic permeability for each membrane tested was calculated by summing the flows through the individual pores and dividing by the total area imaged in the micrograph. An example of our analysis is shown in Figure 2. Figure 2A shows the pore number histogram for a particular membrane, and Figure 2B shows the predicted water flow through each pore in the image. Dagan's formula has been previously validated for micrometer thick membranes with micrometer-sized pores.[15,16] Here we find agreement between the formula and experiment for pnc-Si (Fig-

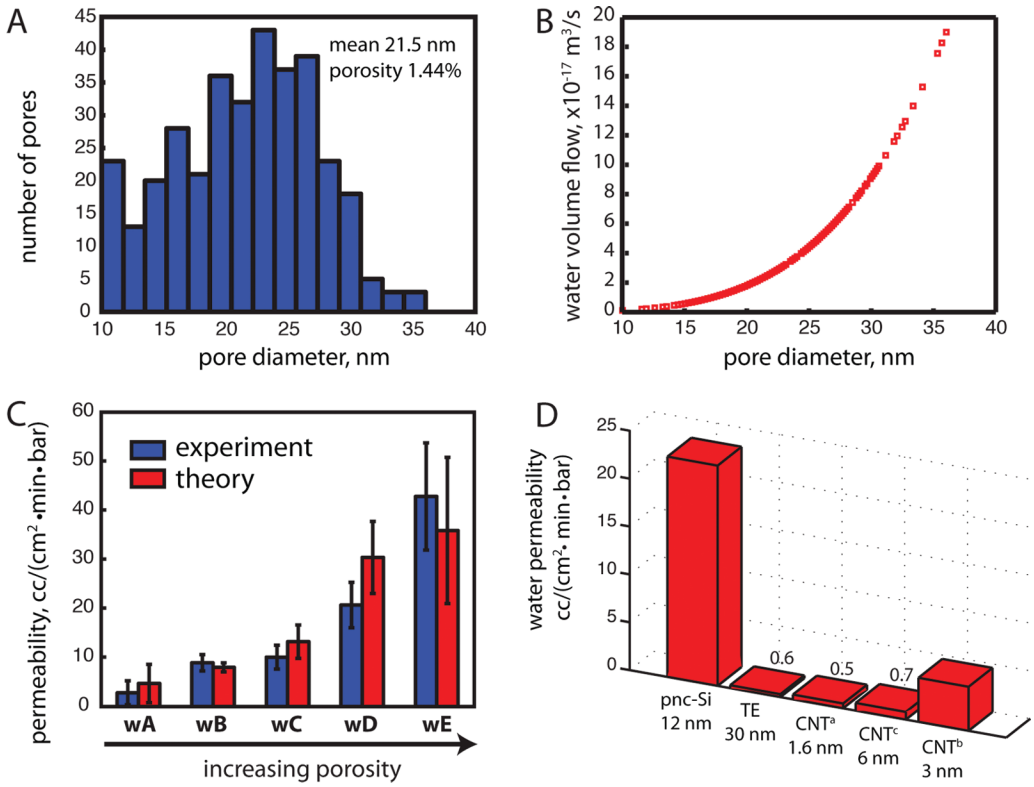

Figure 2. (A) Pore size distribution. The distribution was obtained from a transmission electron micrograph for a particular pnc-Si membrane. (B) Pore-by-pore calculation of theoretical water flow rate through the membrane in (A). The Dagan formula was used to calculate the flow through each pore identified in the TEM image. (C) Experimental and theoretical hydraulic permeability. Membranes from five wafers (labeled wA through wE) were tested experimentally for hydraulic permeability using the device shown in Figure 1C. Data for each wafer were grouped, and error bars reveal the standard deviations for these groups. The error for the theoretical permeability combines the two independent sources of error: processing error and image variability (see Supporting Information). For each wafer, the average porosity, average pore diameter, and number of contributing membranes are as follows: wA = 0.7%, 13.6 nm, *n* = 4; wB = 2.2%, 17.0 nm, *n* = 2; wC = 6.6%, 7.4 nm, *n* = 6; wD = 8.8%, 13.7 nm, *n* = 6; wE = 13.5%, 13.0 nm, *n* = 3. (D) Water permeability of pnc-Si membranes is significantly higher than other nanoporous membranes. Experimentally obtained values for polycarbonate track-etched (TE) membranes agree with manufacturer claims. Data labels: (a) Holt *et al.* Science, 2006; (b) Yu *et al.*, Nano Lett. 2009; (c) Majumder *et al.* Nature 2005. Note: all pore sizes are diameters.

ure 2C), indicating that continuum descriptions of fluids are appropriate for the analysis of flow through these nanometer thick membranes.[16]

In Figure 2D, we compare the hydraulic permeability of a pnc-Si membrane with a 12 nm average pore diameter to the permeabilities of carbon nanotube (CNT) membranes reported in the recent literature to give high flow rates.[17−20] We also compare pnc-Si permeabilities to measurements for commercially available track-etched (TE) membranes assembled into the same centrifuge devices used for pnc-Si hydraulic permeability measurements. Direct comparisons between CNT, TE, and pnc-Si membranes are appropriate given that all three membranes have well-defined through-pores. Advances in manufacturing[21] allowed Yu *et al.* to create CNT membranes with 3 nm pores and ∼80% porosity and achieve hydraulic permeability values of 3.3 cm^3/(cm^2 · min · bar).[20] CNT membranes achieve high hydraulic permeabilities despite being thicker (2−200 μm) and having smaller pores (1−6 nm) than pnc-Si because the smooth and hydrophobic nanotube walls allow fluids to slip.[19,22,23] Unlike CNT membranes, pnc-Si is hydrophilic and the assumption of no-slip, highly viscous flow agrees with measurement (Figure 2). Still, the hydraulic permeability we measure for pnc-Si membranes with 1.4% porosity is 7 times higher than the highest porosity CNT membranes. Not surprisingly, we also found that the hydraulic permeability of pnc-Si membranes is >35-fold higher than 6 μm thick, hydrophilic TE membranes with slightly larger pore sizes (30 nm) and a 3-fold lower porosity (∼0.5% porosity). Indeed, the hydraulic permeability values we report for 15% porous pnc-Si (∼40 mL/(cm^2 · min · bar)) appear to be the highest on record for a nanoporous membrane (pores <100 nm), exceeding commercial ultrafiltration membranes (∼2 mL/(cm^2 · min · bar)),[24] high porosity nanoporous alumina (<1 mL/(cm^2 · min · bar)),[25] experimental block copolymer membranes (∼4 mL/(cm^2 · min · bar)),[26] and 60 nm thick protein membranes (∼15 mL/(cm^2 · min · bar)).[6]

In our initial attempts to measure the hydraulic permeability of pnc-Si, we discovered that membranes are impermeable to water when one side of the membrane is left dry (Figure 3). We explored several strate-

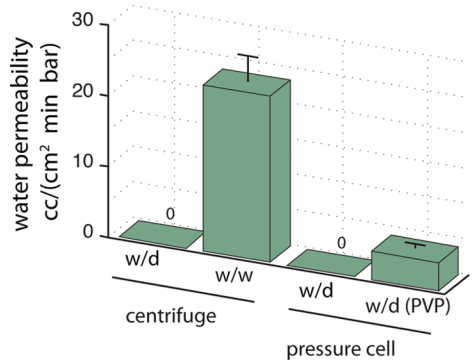

Figure 3. Pnc-Si membranes are impermeable in wet−dry configurations. Pnc-Si membranes were tested for hydraulic permeability in both a centrifuge and in a constant pressure cell. Membranes that are exposed to water on only side are not permeable to water at experimental pressures (0.1−1 bar), while membranes wetted on both sides have significant hydraulic permeability. Membranes coated with hygroscopic PVP were permeable to water when exposed to water on only one side. These samples had an initially lower flow rate, resulting in a lower time-averaged hydraulic permeability over the course of the experiment.

gies to overcome water impermeability of the wet/dry configuration, including the use of high pressures (>1 atm), ozone treatment of membranes to decrease contact angles from ~70 to less than 15° (Figure S2), and lowering surface tension 2−3-fold by adding surfactants (0.2 wt % SDS or 0.2 wt % Triton X-100) or using ethanol instead of water. We also switched from centrifuge-generated pressure to a simple pressure cell because we suspected centrifugal forces were quickly removing fluid droplets from the membrane backside and stopping flow. High water permeability was only observed when we immersed the membrane in water throughout the experiment or added a hygroscopic polymer, polyvinylpyrrolidone (PVP), to the membrane backside. The most reasonable explanation for impermeability of the wet/dry arrangements is that water cannot wick through the pores to wet the backside of a membrane. This is somewhat surprising given that capillary forces should easily drive water to fill 15 nm long hydrophilic pores. While we cannot confirm that the hydrophilic contact angles we measure on the top surface of pnc-Si chips also apply to pore walls, the fact that rapid transmembrane diffusion occurs when the membranes are immersed in water[12,13] does suggest that water has no difficulty entering pores without applied pressure. Thus we suspect that the meniscus in a filled pore cannot advance around the obtuse angles at the pore exit under pressures compatible with pnc-Si membranes.[12]

To examine the performance of pnc-Si membranes in size-exclusion separations, we filtered gold nanoparticles in a size ladder ranging between 5 and 30 nm in diameter. To avoid filtrate dilution from the immersing fluid in the centrifuge setup, we used a simple pressure cell for which flow could be initiated by the addition and removal of 5 μL of water to the membrane backside. The pressure cell was operated at 10 psi until it passed 100 μL of a 200 μL starting sample through membrane chips from three different wafers (**F**, **G**, **H**). Absorbance values in the retentate and filtrate were measured to determine concentrations, and these were normalized to the starting concentration to calculate sieving coefficients. Results show that each pnc-Si membrane exhibited a sharp cut-off with negligible transmission of the larger particle and significant transmission (40−85%) of the smaller particle (Figure 4A). Most notably, membranes from wafer **F** allow more than 80% transmission of 5 nm particles while fully blocking the larger 10 nm nanoparticle (Figure 4A,B). Membranes from wafer **G** also exhibited a resolution of 5 nm, but a cut-off between 10 and 15 nm.

In contrast to pnc-Si, commercially available cellulose (MW cut-offs 3k and 100k) and PES membranes (MW cut-offs 3k, 30k, 50k, 100k) did not pass any nanoparticles between 5 and 30 nm. PES membranes with a reported MW cut-off of 300k did pass nanoparticles in this size range, although passage was clearly hindered as the particle size increased (Figure 4A). This result was surprising as the nominal pore size for 300k ultrafiltration membranes is expected to be ~18 nm[27,28] and suggests the presence of a significant number of larger pores or defects in these "high-flux" membranes. We quantified losses by multiplying concentrations in the retentate and filtrate by the recoverable volumes in each compartment and compared this to the amount of starting material. For pnc-Si, losses were within the experimental uncertainty deriving from pipetting and measurement errors (<5%), while losses were greater than 20% for the 300k PES membranes. Since no detectable quantities of nanoparticles passed into the filtrate and the PES membranes appeared pink after the experiment, the lost particles are presumably embedded in PES membranes. We also performed separation experiments on a protein size ladder containing globular proteins with the exception of a linear myosin control protein (Figure 4D). Table 1 lists the unreduced and reduced sizes of the proteins used in the ladder. The unreduced sizes are relevant to the filtration process, while the reduced sizes are the molecular weights of monomers seen on the reducing gels. The results indicate complete retention of myosin and β-galactosidase (17 nm) and a nearly undiluted transmission of the carbonic anhydrase (~4 nm). The transition between full transmission and full complete retention takes place between olvalbumin (~6.5 nm) and phosphorylase B (8.3 nm), again suggesting a resolution of better than 5 nm for proteins as with nanoparticles.

Using dynamic light scattering, we confirmed that membranes from wafer **G** could be used to "purify" 10 nm particles from a mixture of 10 and 15 nm nanoparticles (Figure 4C). Filtering a mixture of 10 and 15 nm stock largely recovers the light scattering profile of 10 nm nanoparticles with only a slight shift that presum-

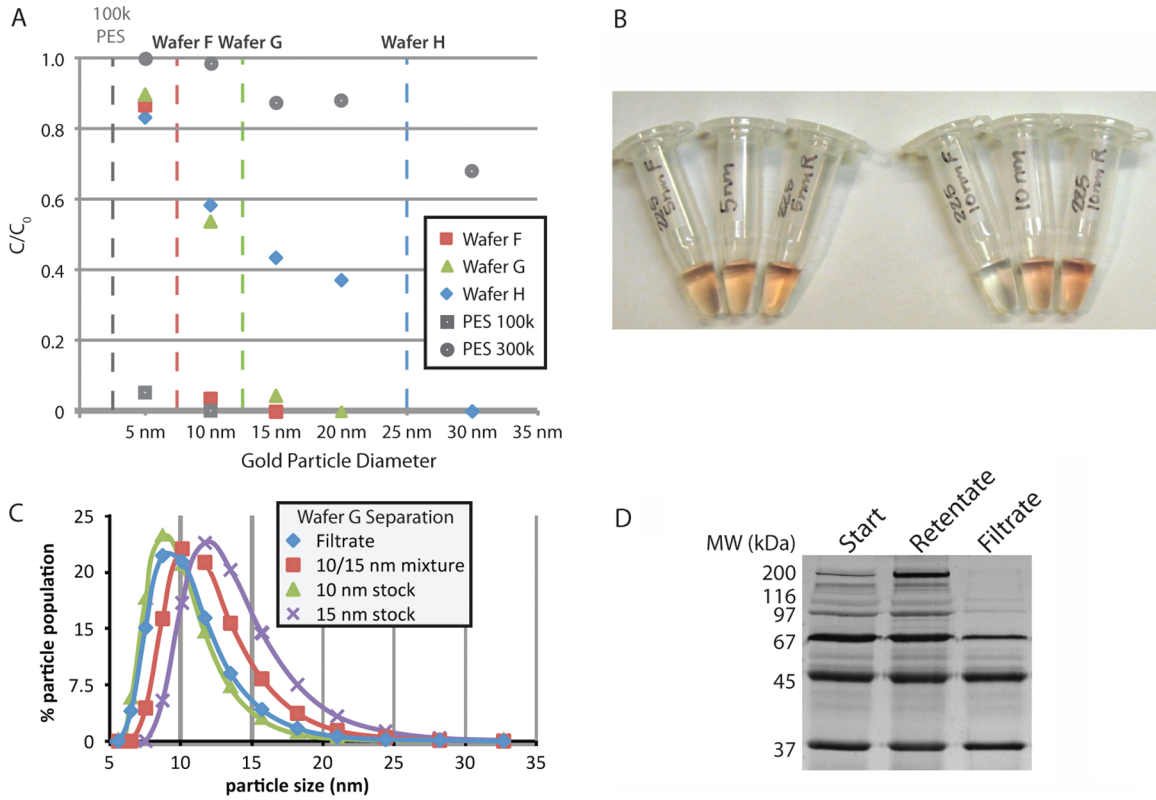

Figure 4. (A) Filtration of gold nanoparticles in a 5−30 nm size ladder. Gold nanoparticle solutions (0.01% solids) were filtered through three different pnc-Si membranes and one commercial PES membrane. Absorbance readings were used to calculate the nanoparticle concentrations and losses. The figure shows the ratio of concentrations in the filtrate *vs* feed solutions as a function of nanoparticle size. Dashed lines are the apparent cut-off for each wafer. (B) Images of stock, retentate, and filtrate solutions for separations with wafer F. Tubes are labeled with particle size and R for retentate, F for filtrate. Stock particles are in the center with no letter designation. (C) Purification of 10 nm particles from a mixture of 10 and 15 nm particles using wafer G. Dynamic light scattering spectra of 15 nm stock gold nanoparticles (black), 10 nm stock (blue), the starting solution containing equal concentrations of 10 and 15 nm particles (green), and the filtrate (red). (D) Fractionation of a protein mixture by SDS−PAGE. The protein size ladder contains six proteins with distinct molecular weights ranging from 37k to 400k when the proteins are in their native state (see Supporting Information for details on protein structure and sizes).

ably arises from some smaller particles in the 15 nm sample entering the filtrate. It is important to note that each nanoparticle stock is not perfectly monodisperse and that light scattering tends to broaden the distribution relative to the actual size of the nanoparticles. We established this by comparing the sizes of nanoparticles in the 10 and 15 nm stocks as measure by light scattering to the sizes of nanoparticles measured by electron microscopy (Table S1). Thus the "purification" of 10 nm particles from the 10 nm/15 nm mixture is implied by fact that the shifted spectrum of the filtered mixture closely resembles the original 10 nm spectrum.

High transmission of materials just below a cut-off is not typical of ultrafiltration membranes[7,29,30] and may be enabled by the thinness of pnc-Si. Advanced sieving theories[31] demonstrate that diffusion can significantly boost the concentration of filtrate materials for ultrathin membranes compared to purely convective transport. The ratio of transport by convection *versus* diffusion is known as the Peclet number:

$$P_e = \frac{VL}{D}$$

where V is the average solvent velocity in a pore, L is the membrane thickness, and D is the diffusion coefficient of the species being transported. For 15 nm thick pnc-Si, $P_e \sim 0.1$, assuming a 4 nm monomeric protein ($D = 1 \times 10^{-6}$ cm^2/s) and a transmembrane velocity of

TABLE 1. Physical Dimensions of Protein in the Size Ladder

molecule	molecular weight of intact molecule	structure	shape	size (nm)	reduced molecular weight
carbonic anhydrase	37000	monomer	globular	4[38]	37000
ovalbumin	45000	monomer	globular	6.5[39]	45000
albumin	67000	monomer	globular	7.5[40]	67000
phosphorylase-B	195000	homodimer	globular	8.3[41]	97000
β-galactosidase	495000	homotetramer	globular	17[42]	116000
myosin II heavy chain	400000	homodimer	linear	160 × 10[43]	200000

0.1 cm/s. By comparison $P_e \sim 3$ for filtration at similar velocities with a commercial ultrafiltration membrane having a 500 nm thick skin. In practice, hindrance from the membrane will increase Peclet numbers because the resistance to solute diffusion through a pore will be greater than the resistance to solute convection through a pore.[32] We estimate that a 12 nm pore would reduce the diffusion coefficient of a 4 nm protein ~6-fold compared to free diffusion and increase P_e to ~0.7 for pnc-Si and to ~20 for conventional membranes. Thus, even after accounting for membrane resistance and despite high velocities within pores, diffusion is a significant contributor for molecularly thin membranes but not for conventional membranes.

The sieving function of pnc-Si is complex and will require more experimentation and advanced modeling to fully understand. For example, the nonlinear dependence of flow rates on pore size (Figure 2B) makes the pore distribution effectively tighter and the cut-off sharper than implied by the physical pore size distribution. We illustrate this with a flow histogram in which we calculate the flow rate through each bin in the pore histogram in Figure 2A (see Figure S3). This analysis shows that the smallest pores contribute very little to the bulk fluid transport and that the transition from the peak flow rates to the largest pore sizes occurs over ~5 nm rather than ~10 nm. We expect that the sharpness of this transition, rather than the breadth of the full pore distribution, is what determines the resolution of the membrane in practice. The magnitude of the membrane cut-off is also not predicted from the physical pore distributions in a straightforward way. In the above experiments, gold nanoparticles were filtered in deionized water so that electrostatic repulsion between the negatively charged particles and the negatively charged membranes will reduce the effective pore sizes. In the case of protein filtration, adsorption is an additional factor known to reduce pore sizes by the thickness of a protein monolayer.[12]

It is important to emphasize that while manufacturing is currently limited to making small membrane devices, the use of highly scalable semiconductor manufacturing allows large numbers of those devices to be made. The membranes used for the current work were produced on 4 inch wafers that contained more than 80 membrane chips. Continued optimization of manufacturing and chip design since the completion of this work is now resulting in more than 400 similar devices being produced on a 6 inch wafer at less than twice the cost (Figure S4). Similarly, while the membranes used in the current work were limited to ~1% active membrane area, which is sufficient to characterize the intrinsic properties of the material, advances in manufacturing are now producing membranes with ~10% active area, which increases the total volumetric flow to ~500 μL/min at 1 atm of pressure. Continued advances in manufacturing, including the use of [110] crystalline silicon to allow vertical etches through the support wafer (rather than the [100] silicon currently used), should allow the fraction of chip area occupied by free-standing membrane to increase at least another 4-fold. Since only standard semiconductor manufacturing processes are used in the production of pnc-Si, the volume of wafers produced each day is also highly scalable. Thus, while the prospects for scaled-up manufacturing of many of the nanoengineered membranes appearing in the literature are dim, large-scale manufacturing is very realisitic and partially achieved already for pnc-Si.

The high hydraulic permeability, sharp size discrimination, scalable fabrication, and low loss characteristics of pnc-Si membranes suggest their immediate use in the purification and production of nanoscale materials. For example, the cut-offs demonstrated here (5−30 nm) can be useful for purifying monomeric proteins from oligomers or for isolating monovalent quantum dots from multivalent dots that induce cross-linking in biological samples.[33] The membranes might also be used for the fractionation of nanoparticles from polydisperse mixtures emerging from batch production.[34] Other membrane-based techniques for high-resolution fractionation of nanoparticles do exist but have important limitations. Hutchison and co-workers purified 1.5 nm gold from a mixture including 3.1 nm gold using commercial ultrafiltration membranes and a diafiltration scheme that resulted in a 15-fold dilution of the smaller species.[35] Dead-end filtration with experimental graft[36] and block[26] copolymer membranes has been shown to provide high-resolution (~5 nm) size discrimination of nanoparticles; however, the pore sizes of these membranes are extremely sensitive to solvent conditions. In contrast, pnc-Si provides high-resolution separations with little dilution of the filtrate and a solvent-independent membrane structure. In a sophisticated process involving buffer and flow optimization, van Reis and colleagues were able to use commercial ultrafiltration membranes in a two-stage, recirculating, tangential flow filtration scheme to separate protein monomers and oligomers with high yield and low dilution.[37] While there is still much to learn about the sieving function of pnc-Si, pnc-Si and other ultrathin membranes hold promise for achieiving similar performance characteristics with simpler filtration schemes.

METHODS

Hydraulic Permeability of Pnc-Si. Custom polypropylene centrifuge housings were designed to hold round formatted silicon chips and were mass-produced by Harbec Inc. (Ontario, NY). Devices were hand assembled by pressing a polypropylene retention ring against a pnc-Si chip and a 5 mm Viton O-ring placed at the base of the housing. The assembled devices and a round-bottom 10 mL test tube were both weighed before the experiment.

In wet/wet experiments, 500 μL of distilled and deionized water was added to both the insert and the test tube. Before inserting the device into the centrifuge tube, a 30 μL droplet of water from the tube was added to the backside of the membrane to prevent an air bubble from forming beneath the membrane during immersion. The top of the centrifuge tube was sealed to prevent evaporation, and the tube was placed in a centrifuge and spun for 30−60 min at 75 rcf. After the experiment was finished, the insert was removed from the test tube. Any remaining water on the backside of the insert was removed and added back into the tube. The tube and insert final weights were subtracted from initial values to determine the volume of water in each. In most experiments, 100−200 μL of deionized water passed through the membrane over the course of 30−60 min of centrifugation. Control experiments with broken membranes gave hydraulic permeability values at least one order higher than those measured for intact pnc-Si, and control experiments with solid silicon frames detected no leaks.

In order to generate fluid flow without membrane immersion, we treated the membrane backside with polyvinylpyrrolidone (PVP, Sigma Aldrich, St. Louis, MO). Three microliters of 1 mg/mL PVP in methanol (w/v) was pipetted onto the backside of a membrane. The membrane was allowed to dry for a minimum of 2 h under ambient conditions. The membrane was assembled into the pressure cell with 500 μL of deionized water in the feed tube. The pressure was held constant at 3 psi for 30 min, and the water on the backside was collected and measured on a balance. Initial flow rates were low, likely due to a delay in the wetting process. This could explain the low calculated hydraulic permeability values for PVP-treated membranes compared to wet/wet format. After these experiments with PVP confirmed that the difficulty with wet/dry configuration was the lack of wetting on the membrane backside, we found that adding and removing droplets of water from the backside without PVP could be used to initiate flow in the pressure cell, although again the flow did not immediately rise to its peak values. For these reasons, we preferred the centrifuge setup for hydraulic permeability studies. On the other hand, the pressure cell provided an advantage for separation studies because it did not require an immersing fluid that results in filtrate dilution. We verified that the flow of DI water through the pnc-Si membranes in the pressure cell was time-independent (Figure S5).

Hydraulic Permeability of Track-Etched Membranes. Commercially available polycarbonate track-etched membranes (Sterlitech) were cut into circular discs with a diameter of 0.70 cm (0.38 cm^2 area) using a custom pressure die. In order to test the hydraulic permeability of these membranes in a centrifuge setup, centrifuge filter units from Millipore (Microcon) were disassembled with slight application of pressure. The regenerated cellulose membranes were replaced with the previously cut polycarbonate track-etched membranes, and the Microcon devices were then reassembled. Centrifugation was performed with the same initial pressures as in the pnc-Si experiments for between 10 and 30 min. Graphs of volume passed through the membrane over time were created, and the hydraulic permeability was calculated from the extrapolated initial slope of these curves.

Membrane Production. Pnc-Si membranes were fabricated as previously described.[12] Briefly, a 1000 Å thermal oxide was grown on both sides of a (100) N-type silicon wafer. The backside of the wafer was patterned using photolithography in order to form an etch mask for the nanocrystalline membranes. After lithography, the front side oxide was removed. A three-layer silicon dioxide (20 nm)/amorphous silicon (15 nm)/silicon dioxide (20 nm) film stack was then deposited onto the bare silicon wafer by RF magnetron sputtering (AJA International, North Scituate, MA). The deposition rates for the silicon dioxide and amorphous silicon layers are well-characterized.[12] Pores were formed by inducing a phase transition in the silicon layer from an amorphous to nanocrystalline state using a rapid thermal annealing process ranging from 850 to 1100 °C (Surface Science Integration, El Mirage, AZ). The membrane was released by etching the backside of the silicon wafer with a preferential silicon etchant, ethylenediamine pyrocatechol (EDP). Due to its high silicon to oxide etch selectivity, the EDP etch terminated at the first protective oxide layer in the membrane film stack. Finally, the protective oxide layers were etched with buffered oxide etchant (BOE), thus exposing the porous nanocrystalline silicon membrane. The mask was designed to yield 84 samples per silicon wafer. Each sample contained two 2000 μm × 100 μm slits with free-standing 15 nm thick pnc-Si membranes.

Electron Microscopy. Plan-view transmission electron microscopy of pnc-Si membranes was performed in bright-field mode at 80 kV using a Hitachi H-7650 transmission electron microscope (TEM). Membranes were formatted on each wafer to be compatible with the TEM specimen holder. Images were acquired with an Olympus Cantega 11 megapixel digital camera.

Pore Image Processing and UV/Ozone Treatments. See legends of Supporting Information Figures S1 and S2.

Gold Nanoparticle Filtration. Stock solutions (0.01% w/v) of gold nanoparticles (British BioCell International, Cardiff, UK) were diluted 1:1 with ddH_2O. Two hundred microliters of diluted gold was placed in assembled plastic housings with pnc-Si membranes and pressurized to 10 psi using a pressure cell described above. Pressure was maintained until approximately one-half of the volume passed through the membranes (typically 5−15 min). The retentate and filtrate solutions were recovered and weighed to determine total volume recovery, which was typically 198 μL. The retentate solution was pipetted up and down against the membrane five times to maximize recovery of gold that had settled against the membrane. The peak absorbance between 500 and 550 nm of the retentate and filtrate was measured on a NanoQuant plate using a Tecan plate reader (Tecan Group, Männedorf, Switzerland) and compared to stock solution peak values. Using the volume and concentrations of the retentate and filtrate, percent nanoparticle recovery was calculated. To perform a separation of 10 and 15 nm gold (Figure 4C), equal parts of stock solutions were mixed without ddH_2O dilution.

Pall Nanosep filtration devices with PES membranes (Pall, Port Washington, NY) were tested in our pressure cell using a similar approach. Two hundred microliters of diluted gold was pressurized at 10 psi until approximately one-half of the volume passed through the filter. Like with pnc-Si membranes, the retentate solution was recovered by pipetting up and down against the membrane five times to maximize recovery. In most cases, a light pink color remained in the membrane even after vigorous pipetting, likely accounting for the reduced recovery percentages compared to pnc-Si.

Millipore Microcon filtration devices with cellulose membranes (Millipore, Billerica, MA) were also tested, but since Millipore devices could not easily be adapted to our pressure cell, separation experiments were performed in a fixed rotor centrifuge at 14 000 rcf according to manufacturer's instructions. All of the cellulose membranes tested (3k, 30k, 50k, and 100k rated molecular weight cut-off) retained all of the gold species.

Protein Separations. One hundred microliters of a 1 mg/mL total protein mixture containing myosin, β-galactosidase, phosphorylase B, albumin, ovalbumin, and carbonic anhydrase in PBS was loaded into the plastic housing and pressurized at 2 psi for 40 min. The backside of the membrane was prewet with 10 μL of PBS to initiate flow. Ten microliters of the filtrate was removed from the backside of the membrane and prepared for SDS−PAGE along with the starting solution and remaining feed solution (retentate). Silver stain was used to visualize proteins on the completed gels. The molecular weight and other physical properties of the proteins are given in Table 1. Note that the MW of the nonreduced (intact) molecules being filtered is different than the MW shown on the reducing gel in Figure 4D. Sizes are approximate based on crystal dimensions with the exception of myosin, which is taken from EM data.

Acknowledgment. Financial support for this work was provided by NIH 1R21EB006149, NSF DMR0722653, and NSF ECCS0707795 and by a seed grant from the Johnson and Johnson Discovery Fund. The authors wish to acknowledge Mike Bindschadler's work on the pore processing program (available for download at http://nanomembranes.org/resources/software/) and Dr. Jan Ho (Johns Hopkins University) who provided insight on the impermeability of wet/dry configurations.

Supporting Information Available: Analysis of hydraulic permeability in wet/wet configurations; estimates of uncertainty in predicting hydraulic permeability; supplemental figures explaining pore processing and UV/ozone treatments; supplemental figure showing progress on scaled-up manufacturing of pnc-Si membranes; supplemental figure showing time water flow through pnc-Si chips is not time dependent; table of nanoparticle sizes determined by transmission electron microscopy and dynamic light scattering. This material is available free of charge *via* the Internet at http://pubs.acs.org.

As founders of SiMPore Inc., J.L.M., T.R.G., P.M.F., and C.S.S. declare a competing financial interest in this work.

REFERENCES AND NOTES

1. Ghosh, R. Protein Separation Using Membrane Chromatography: Opportunities and Challenges. *J. Chromatogr. A* **2002**, *952*, 13–27.
2. Bhut, B. V.; Husson, S. M. Dramatic Performance Improvement of Weak Anion-Exchange Membranes for Chromatographic Bioseparations. *J. Membr. Sci.* **2009**, *337*, 215–223.
3. Bhut, B. V.; Wickramasinghe, S. R.; Husson, S. M. Preparation of High-Capacity, Weak Anion-Exchange Membranes for Protein Separations Using Surface-Initiated Atom Transfer Radical Polymerization. *J. Membr. Sci.* **2008**, *325*, 176–183.
4. Ghosh, R. Rapid Antibody Screening by Membrane Chromotagraphic Immunoassay Technique. *J. Chromatogr. B* **2006**, *844*, 163–167.
5. Wang, Y.; Balgley, B. M.; Rudnick, P. A.; Evans, E. L.; DeVoe, D. L.; Lee, C. S. Integrated Capillary Isoelectric Focusing/Nano-Reversed Phase Liquid Chromatography Coupled with ESI-MS for Characterization of Intact Yeast Proteins. *J. Proteome Res.* **2005**, *4*, 36–42.
6. Peng, X.; Jin, J.; Nakamura, Y.; Ohno, T.; Ichinose, I. Ultrafast Permeation of Water through Protein-Based Membranes. *Nat. Nanotechnol.* **2009**, *4*, 353–357.
7. Cheryan, M. *Ultrafiltration Handbook*; Technomic Publishing Co: Lancaster, PA, 1986.
8. Martin, C. R.; Siwy, Z. Molecular Filters: Pores within Pores. *Nat. Mater.* **2004**, *3*, 284–295.
9. Fissell, W. H.; Dubnisheva, A.; Eldridge, A. N.; Fleischman, A. J.; Zydney, A. L.; Roy, S. High-Performance Silicon Nanopore Hemofiltration Membranes. *J. Membr. Sci.* **2009**, *326*, 58–63.
10. Tong, H.; Jansen, H.; Gadgil, V.; Bostan, C.; Bereschot, E.; van Rijin, C.; Elwenspoek, M. Silicon Nitride Nanosieve Membrane. *Nano Lett.* **2004**, *4*, 283–287.
11. Vlassiouk, I.; Apel, P. Y.; Dmitriev, S. N.; Healy, K.; Siwy, Z. S. Versatile Ultrathin Nanoporous Silicon Nitride Membranes. *Proc. Natl. Acad. Sci. U.S.A.* **2009**, *106*, 21039–21044.
12. Striemer, C. C.; Gaborski, T. R.; McGrath, J. L.; Fauchet, P. M. Charge- and Size-Based Separation of Macromolecules Using Ultrathin Silicon Membranes. *Nature* **2007**, *445*, 749–753.
13. Kim, E.; Xiong, H.; Striemer, C. C.; Fang, D. Z.; Fauchet, P. M.; McGrath, J. L.; Amemiya, S. A Structure-Permeability Relationship of Ultrathin Nanoporous Silicon Membrane: A Comparison with the Nuclear Envelope. *J. Am. Chem. Soc.* **2008**, *130*, 4230–4231.
14. Dagan, Z.; Weinbaum, S.; Pfeffer, R. An Infinite-Series Solution for the Creeping Motion through an Orifice of Finite Length. *J. Fluid Mech.* **1982**, *115*, 505–523.
15. Dushman, S. *Scientific Foundations of Vacuum Technique*, 2nd ed.; John Wiley & Sons: New York, 1962.
16. Kusmanto, R.; Jacobsen, E.; Finlayson, B. Applicability of Continuum Mechanics to Pressure Drop in Small Orifices. *Phys. Fluids* **2004**, *16*, 4129–4134.
17. Hinds, B. J.; Chopra, N.; Rantell, T.; Andrews, R.; Gavalas, V.; Bachas, L. G. Aligned Multiwalled Carbon Nanotube Membranes. *Science* **2004**, *303*, 62–65.
18. Majumder, M.; Chopra, N.; Andrews, R.; Hinds, B. J. Nanoscale Hydrodynamics: Enhanced Flow in Carbon Nanotubes. *Nature* **2005**, *438*, 44.
19. Holt, J. K.; Park, H. G.; Wang, Y.; Stadermann, M.; Artyukhin, A. B.; Grigoropoulos, C. P.; Noy, A.; Bakajin, O. Fast Mass Transport through Sub-2-Nanometer Carbon Nanotubes. *Science* **2006**, *312*, 1034–1037.
20. Yu, M.; Funke, H. H.; Falconer, J. L.; Noble, R. D. High Density, Vertically-Aligned Carbon Nanotube Membranes. *Nano Lett.* **2009**, *9*, 225–229.
21. Futaba, D. N.; Hata, K.; Yamada, T.; Hiraoka, T.; Hayamizu, Y.; Kakudate, Y.; Tanaike, O.; Hatori, H.; Yumura, M.; Iijima, S. Shape-Engineerable and Highly Densely Packed Single-Walled Carbon Nanotubes and Their Application as Super-Capacitor Electrodes. *Nat. Mater.* **2006**, *5*, 987–994.
22. Hummer, G.; Rasaiah, J. C.; Noworyta, J. P. Water Conduction through the Hydrophobic Channel of a Carbon Nanotube. *Nature* **2001**, *414*, 188–190.
23. Sokhan, V. P.; Nicholson, D.; Quirke, N. Transport Properties of Nitrogen in Single Walled Carbon Nanotubes. *J. Chem. Phys.* **2004**, *120*, 3855–3863.
24. Millipore Corporation. 2008. Product Selection Guide: Ultrafiltration Selection Guide. Available at http://www.millipore.com/techpublications/tech1/Pf1172en00.
25. Thormann, A.; Teuscher, N.; Pfannmoller, M.; Rothe, U.; Heilmann, A. Nanoporous Aluminum Oxide Membranes for Filtration and Biofunctionalization. *Small* **2007**, *3*, 1032–1040.
26. Schacher, F.; Ulbricht, M.; Muller, A. Self-Supporting, Double Stimuli-Responsive Porous Membranes from Polystyrene-Block-Poly(*N*,*N*-dimethylaminoethyl methacrylate) Diblock Copolymers. *Adv. Funct. Mater.* **2009**, *19*, 1040–1045.
27. Latulippe, D. R.; Ager, K.; Zydney, A. L. Flux-Dependent Transmission of Supercoiled Plasmid DNA through Ultrafiltration Membranes. *J. Membr. Sci.* **2007**, *294*, 169–177.
28. Latulippe, D. R.; Zydney, A. L. Salt-Induced Changes in Plasmid DNA Transmission through Ultrafiltration Membranes. *Biotechnol. Bioeng.* **2008**, *99*, 390–398.
29. Zeman, L.; Wales, M. Polymer Solute Rejection by Ultrafiltration Membranes. In *Synthetic Membranes*; Turbak, A. F., Ed.; American Chemical Society: Washington, DC, 1981; Vol. 2.
30. Michaels, A. S. Analysis and Prediction of Sieving Curves for Ultrafiltration Membranes: A Universal Correlation. *Sep. Sci. Technol.* **1980**, *15*, 1305–1322.
31. Mochizuki, S.; Zydney, A. L. Theoretical Analysis of Pore Size Distribution Effects on Membrane Transport. *J. Cell Sci.* **1993**, *82*, 211–227.
32. Dechadilok, P.; Deen, W. Hindrance Factors for Diffusion and Convection in Pores. *Ind. Eng. Chem. Res.* **2006**, *45*, 6953.
33. Howarth, M.; Liu, W.; Puthenveetil, S.; Zheng, Y.; Marshall, L. F.; Schmidt, M. M.; Wittrup, K. D.; Bawendi, M. G.; Ting, A. Y. Monovalent, Reduced-Size Quantum Dots for Imaging Receptors on Living Cells. *Nat Methods* **2008**, *5*, 397–399.
34. Yen, B.; Stott, N.; Jensen, K.; Bawendi, M. A Continuous-Flow Microcapillary Reactor for the Preparation of a Size-Series of CdSe Nanocrystals. *Adv. Mater.* **2003**, *15*, 1858–1862.
35. Sweeny, S.; Woehrle, G.; Hutchinson, J. Rapid Purification and Size Separation of Gold Nanoparticles *via* Diafiltration. *J. Am. Chem. Soc.* **2006**, *128*, 3190–3197.
36. Akthakul, A.; Hochbaum, A.; Stellacci, F.; Mayes, A. Size Fractionation of Metal Nanoparticles by Membrane Filtration. *Adv. Mater.* **2005**, *17*, 532–535.
37. van Reis, R.; Gadam, S.; Frautschy, L. N.; Orlando, S.; Goodrich, E. M.; Saksena, S.; Kuriyel, R.; Simpson, C. M.; Pearl, S.; Zydney, A. L. High Performance Tangential Flow Filtration. *Biotechnol. Bioeng.* **1997**, *56*, 71–82.
38. Saito, R.; Sato, T.; Ikai, A.; Tanaka, N. Structure of Bovine Carbonic Anhydrase II at 1.95 Å Resolution. *Acta Crystallogr., Sect. D* **2004**, *60*, 792–795.

39. Stein, P. E.; Leslie, A. G.; Finch, J. T.; Carrell, R. W. Crystal Structure of Uncleaved Ovalbumin at 1.95 Å Resolution. *J. Mol. Biol.* **1991**, *221*, 941–959.
40. Sugio, S.; Kashima, A.; Mochizuki, S.; Noda, M.; Kobayashi, K. Crystal Structure of Human Serum Albumin at 2.5 Å Resolution. *Protein Eng.* **1999**, *12*, 439–446.
41. Gregoriou, M.; Noble, M. E.; Watson, K. A.; Garman, E. F.; Krulle, T. M.; de la Fuente, C.; Fleet, G. W.; Oikonomakos, N. G.; Johnson, L. N. The Structure of a Glycogen Phosphorylase Glucopyranose Spirohydantoin Complex at 1.8 Å Resolution and 100 K: The Role of the Water Structure and Its Contribution to Binding. *Protein Sci.* **1998**, *7*, 915–927.
42. Juers, D. H.; Jacobson, R. H.; Wigley, D.; Zhang, X. J.; Huber, R. E.; Tronrud, D. E.; Matthews, B. W. High Resolution Refinement of β-Galactosidase in a New Crystal Form Reveals Multiple Metal-Binding Sites and Provides a Structural Basis for α-Complementation. *Protein Sci.* **2000**, *9*, 1685–1699.
43. Elliott, A.; Offer, G.; Burridge, K. Electron Microscopy of Myosin Molecules from Muscle and Non-Muscle Sources. *Proc. R. Soc. London, Ser. B* **1976**, *193*, 45–53.